Journal of Structural Geology 190 (2025) 105291

Contents lists available at ScienceDirect

Journal of Structural Geology

journal homepage: www.elsevier.com/locate/jsg

# Geometry of curved slickenlines as a function of rupture direction, asperity durability and coseismic roughening of fault surfaces

Timothy A. Little [a,*], Jesse Kearse [a], Yoshi Kaneko [b], Russ Van Dissen [c]

[a] Victoria University of Wellington, P. O. Box 600, 6140, Wellington, New Zealand
[b] Kyoto University, Kitashirakawa, Oiwake-cho, Sakyo-ku, 606-8502, Kyoto Japan
[c] GNS Science, P. O. Box 30-368, 5040, Lower Hutt, New Zealand

ARTICLE INFO

*Keywords:*
Dynamic stresses
Curved slickenlines
Slickenline patterns
Earthquake propagation direction
Fault surface roughness evolution

ABSTRACT

Global data indicate slickenlines inscribed during surface rupturing earthquakes are typically curved. Dynamic rupture modelling relates slip curvature to time-varying stresses in rupture process zones. Such models generate striation curvature depending on rupture propagation direction and Andersonian slip type. Using 2D kinematic models in a new MATLAB program called *Slicks*, we explore expected patterns of curved slickenline on fault surfaces, comparing them to observations of natural slip striae on scarps of the Kekerengu Fault after the 2016 Kaikōura Earthquake, New Zealand, and the Alpine Fault, New Zealand which last ruptured in 1717 CE. As predicted by the dynamic rupture models, some slickenlines on both faults are curved at their upstream (older) ends and transition downstream to a longer, straighter trajectory. *Slicks* predicts that curved tracks should intersect, a relationship that we observed in the field, and that, for a given slip history, slickenline patterns and track-length distributions should vary depending on initial density of plowing elements, their mean durability or longevity, and the rates at which new asperities are introduced and smoothed. Striation patterns on the Kekerengu Fault suggest that inscribing asperities were established at the beginning of the earthquake rupture, with this roughness being quickly smoothed during the earthquake.

## 1. Introduction

Most slickenlines (slip striae) exposed on the scarps of historic earthquake ruptures are either curved or misaligned to the finite (coseismic) slip vector defined by the 3D offset of nearby landforms or cultural features (Kearse and Kaneko, 2020, and references therein). Dynamic rupture models predict that the curvature of coseismic slip directions in the near surface will be influenced by the direction of propagation of earthquake rupturing through a site, and to be the result of elastic stress changes in the process zone of that rupture (Spudich et al., 1998; Kearse et al., 2019; Kearse and Kaneko, 2020; Macklin et al., 2021; Aoki et al., 2023). So far, dynamic rupture models have been benchmarked against the curved shape of slickenlines on eight historic earthquake ruptures for which hypocentral locations and focal mechanisms are instrumentally known; these include strike-slip, normal, reverse and oblique-slip examples (Kearse and Kaneko, 2020). Slickenline curvature potentially provides a valuable new tool in seismic hazard evaluation, because rupture propagation direction exerts a fundamental control on the intensity of seismic shaking at a site (e.g., Somerville et al., 1997), yet remains difficult to discern in the paleoseismic record (but see Howarth et al., 2021). Because of the sparsity of information regarding past propagation directions, it is difficult to establish whether or not large-magnitude earthquakes tend to repeat a particular rupture direction.

At depths of just a few meters along a ground-surface rupture (where normal stresses and temperatures are low, and strength contrasts are high), grooves on fault surfaces at the cm-m scale are generally interpreted to form as a result of hard asperities (indentors or plowing elements) raking across softer material on the opposite block to cause localized frictional failure and abrasional wear (e.g., Means, 1987; Petit, 1987; Doblas, 1998; Candela et al., 2012; Tjia, 2014; Scholz, 2019). Where that softer material is gouge, soil, or unconsolidated wall rocks, that failure may involve granular flow; moreover, the accumulation and streaking of granular fault rock may contribute to striation formation (Doblas, 1998; Tjia, 2014; Tesei et al., 2017; Brodsky et al., 2020). Curved slickenlines are commonly observed in the near-surface along

* Corresponding author. School of Geography, Environment and Earth Sciences, New Zealand.
*E-mail addresses:* timothy.little@vuw.ac.nz (T.A. Little), jesse.kearse@vuw.ac.nz (J. Kearse), kaneko.yoshihiro.4e@kyoto-u.ac.jp (Y. Kaneko), r.vandissen@gns.cri.nz (R. Van Dissen).

https://doi.org/10.1016/j.jsg.2024.105291
Received 12 May 2024; Received in revised form 4 November 2024; Accepted 11 November 2024
Available online 13 November 2024

active faults and are less common along originally deeper (but now exhumed) fault plane (Kearse and Kaneko, 2020). In this paper, we briefly summarize the results of dynamic rupture models, especially their predictions for patterns of slickenline curvature as a function of source mechanism, rupture propagation direction, fault rheological parameters, and local fault geometry. We use a new 2D MATLAB program called *Slicks* to simulate curved slickenline tracks on fault surfaces, focusing on their resulting shapes, intersections of with another, and potential diversity of track-length distributions. Purely kinematic, the program is used to forward-model slickenline patterns based on a prescribed slip path or history that can be in part curved. We show how for a given slip path, track patterns and length distributions should vary in a predictable way because of differences in the relative rates of asperity production versus removal during an earthquake. We also suggest how best to use field observations of curved or intersecting slickenline tracks to infer the propagation direction of past earthquake ruptures, including where on a scarp early-formed, curved tracks are most likely to be preserved.

Past research has focused on quantitative description of fault surface roughness across a broad spectrum of spatial observational scales, including the typical mm-cm width and depth of slickenlines that are typically seen in the field. These studies have led to interpretations regarding the processes that may control the evolution of this roughness, and their impact on fault mechanical properties (e.g., Boneh et al., 2014; Brodsky et al., 2016). A particular gap in knowledge is what fault roughness changes may occur during a single seismic-slip event (meters of slip, seconds of time) (e.g., Brodsky et al., 2011; Shervais and Kirkpatrick, 2016). Depending on the setting (e.g., depth, pressure, observational length scale, time frame), faults are commonly inferred to get smoother as they accrue slip (e.g., Wesnousky, 1989; Brodsky et al., 2011; Badt et al., 2016; Perrin et al., 2021) or perhaps to achieve a steady-state pattern of fault surface roughness (Candela et al., 2012). We argue that after a ground-surface rupturing earthquake, field-based documentation of slickenline patterns on coseismically exposed scarps can be used to estimate how much fault slip, on average, a slickenline-inscribing asperity can survive before it is removed; and how frequently new asperities may nucleate as a function of continuing coseismic slip. Furthermore, the shape and length patterns of slickenline striations may provide valuable information regarding the timing (early vs late) of fault roughening versus fault smoothing (asperity creation or removal) processes on a fault during a slip of known magnitude.

To benchmark our modelling predictions against field examples, we briefly describe the geometry of slickenlines that formed along the active Kekerengu Fault during the Mw 7.8 2016 Kaikōura Earthquake, New Zealand. During this NE-propagating rupture, the predominantly dextral-slip fault slipped laterally by up to ~12 m, and inscribed variably curved slickenlines on coseismically exhumed fault scarps (Kearse et al., 2018, 2019). For an additional field example, we also describe curved slickenline tracks observed on slip surfaces of the active Alpine Fault (Barth et al., 2024).

## 2. Models for origin of curved fault-slip trajectories

Prior to recent dynamic rupture modelling studies, the origin of curved fault slip had been explained in several ways. We summarize these, below. Using a kinematic computer model, Mandal and Chakraborty (1989) showed that a rigid-body fault block rotation will generate a population of curved slickenlines of variable shapes and lengths, depending on a particular site's distance from axis of rotation, which is assumed to be fault-orthogonal; whereas curved, non-rotational slip trajectories involving a continuously variable rake direction will generate slickenlines of similar shape to one another on different parts of the same fault. The similar shape, lengths, and complexity of slickenlines observed on different parts of natural earthquake ruptures rules out the first of these suggested options (Kearse and Kaneko, 2020). Another mechanism to generate curved slickenlines is rigid rotation of fault-blocks relative to a fixed regional stress tensor. In this situation, shear traction vectors resolved on a rotating fault plane would progressively change their orientation, thus potentially leading to curved slickenline tracks (Xu et al., 2011). A variant of this model (more applicable to shear zones) considers small blocks that are "micro--rotating" as a result of vorticity in a rock volume that is undergoing a non-coaxial bulk deformation. The direction of maximum shear-strain rate as resolved on the fault planes bounding these small rotating blocks changes orientation and thus may lead to curved tracks (Twiss and Gefell, 1990). Fault-block rotational mechanisms cannot explain the marked curvature (i.e., >30° of deflection) of natural slickenlines on fault surfaces that formed during coseismic slip increments of only a few metres (Kearse and Kaneko, 2020).

Doblas and Rubio (1987) suggest that differential strain accumulation in opposing fault blocks through time (different "absolute motions") can lead to the development of curved slickenlines along their fault boundary, but this is a ductile rather than seismogenic process and cannot explain curved racks on fault scarps. Another model posits that varying slip orientations on a fault reflects stress perturbations caused by seismic events on nearby crustal-scale faults through elastic fault interactions near their tips or intersections (Cashman and Ellis, 1994; Maerton, 2000; Xu et al., 2013). In these models, after a given slip increment on one fault, the magnitude of shear traction rake change on the other fault should depend on the relative attitudes and positions of two faults, their aspect ratios, and Poisson's ratio; depending on these, a deflection in slip direction by as much as ~30° might occur (Maerton, 2000). Note that this last mechanism can explain abrupt changes in slip direction as a result of multiple rupture events on a set of adjacent faults but not a smooth and continuous curving of slickenlines on a single fault during one earthquake.

Now we briefly review recent studies that simulate coseismic slip-direction curvature that are based on dynamic rupture models. Of general applicability, the models have been shown to be successful at predicting the observed local sense of curvature of slickenlines on historic earthquake scarps as a function of the type of fault rupture and its local direction of propagation (Kearse et al., 2019; Kearse and Kaneko, 2020; Aoki et al., 2023). The models simulate the spontaneous, dynamic rupture of a single crustal-scale fault, typically in a 3D homogeneous elastic half-space, using a spectral-element code (Kaneko et al., 2008). Prior to a simulated earthquake, the fault is at rest and subject to uniform regional stresses that increase linearly with depth. An earthquake is seeded on a patch in the central part of the fault at 7–12 km down-dip distance, after which the rupture propagates along the fault surface according to slip-weakening friction laws. Key input variables include the initial stress system (i.e., strike-slip, reverse, or normal Andersonian regime); the fault attitude and shape; the P- and S-wave velocities; the characteristic slip distance (Dc) over which the static friction (μs) decreases linearly to its dynamic value (μd); and the fault frictional cohesion (C), which is taken to increase linearly with depth. During the earthquake, the slip-velocity is assumed to remain parallel to the shear traction vector at all fault nodes. For a more detailed description of the modelling and its assumptions see Aoki et al. (2023).

According to dynamic rupture models, the curved part of the track is inscribed during the earliest phase of slip when the pulse of transient elastic stresses in the rupture process zone propagates across the site, generally affecting <20% of the total slip path length. Over a wide range of the above-cited input variables, the local sense and direction of convexity of the coseismic slip-path on a fault is chiefly governed by a site's location relative to the propagating rupture, and the direction and polarity of the pre-rupture shear traction on the fault (i.e., the faulting regime). Dynamic stresses generated in the process zone at the rupture tip induce transient stresses on the fault surface that are not parallel to initial (static) shear traction direction, and temporal changes in these stresses drive a gradational change in the rake of the slip direction. With time, the dynamic stresses dissipate, allowing the shear traction to transition back towards its pre-stress direction, leaving in its wake a

curved slickenline trace.

For a strike-slip rupture, the local dynamic stresses near the rupture tip introduce vertical stress components (uplift on one side, subsidence on the other) that are large enough to drive a rapid early pulse of partly dip-slip motion on the fault (Fig. 1). Importantly, these pulses are of opposite polarity (sense of dip-slip) at opposite ends of the rupture (Fig. 1). After the rupture front has passed (e.g. at time >5–6 s in Fig. 1), the vertical stresses wane, slip becomes subhorizontal and the rate of net slip decreases. The models predict that the amplitude of slip-rate deflection (i.e., slickenline curvature) is greatest at the ground surface, and that it decreases rapidly with depth below that level (Kearse et al., 2019, e.g., their Fig. 3C). This depth-related damping effect reflects the following: at the free surface the dynamic stresses are large relative to the confining pressure and pre-stress magnitudes (both of which are essentially zero), whereas at depth the opposite is true. In Fig. 1, this damping effect is depicted by the downward gradient in colors (coded to slip rakes) from the ground surface. The models suggest that coseismic slip-vector deflection away from the pre-stress traction direction reduces to <1° at depths below ~3 km (e.g., Kearse et al., 2019). This depth dependency may explain why curved slickenline tracks are common on earthquake scarps, but seemingly uncommon on the surface of more deeply exhumed faults. Fig. 1 illustrates that the sites of maximum dynamic stress magnitude and slip-vector deflection occur adjacent to the intersections of the rupture front with the ground surface. There, the rupture tip lines are neither horizontal or vertical, but are inclined and mixed mode (II + III). For Andersonian stress states (e.g., Fig. 1), the tip lines at opposite ends of the rupture are predicted to be symmetrical, plunging away from each other at equal angles relative to the horizontal (Kearse and Kaneko, 2020).

Based on dynamic rupture modelling, patterns of slickenline curvature on natural faults can be used to infer the direction of rupture propagation (earthquake directivity) at a site. Fig. 2A–D depict expected senses of slip-vector curvature on opposite sides of a bilaterally propagating rupture for end-member cases of Andersonian faults. Note that the sense of slickenline convexity at a site depends on which fault block is being observed (compare red vs. black arrows in Fig. 2). If an earthquake rupture is oblique-slip (i.e., intermediate between two Andersonian end-members), then the two tip lines on either side of a ground rupture no longer plunge away from each other at equal angles. In this more asymmetrical situation, the senses of slip path convexity on either side of a rupture remain opposite, but the local magnitudes of deflection are no longer equal. The tip line that is most mixed-mode in character (i.e., closest to 45° in its plunge) hosts the largest magnitude of dynamically-induced slip path deflection at the ground surface (Aoki et al., 2023).

The above-cited modelling studies assume a planar fault with uniform fault friction parameters embedded in an elastic homogeneous medium. Natural faults are more complex than this. Aoki et al. (2023) simulated dynamic ruptures on nonplanar faults; in particular, vertical strike-slip faults that locally bend along strike into secondary, oblique-slip fault segments that are non-vertical. For most of their model runs the local sense of curvature of the slip paths on the main and secondary faults are the same and show the same relationships as those depicted in Fig. 2. This accordance reflects the fact that a modelled rupture is many kilometers in spatial dimension, and that both faults (main, secondary) are overprinted by a similar temporal change in dynamic stresses during rupture passage. Thus their slip paths are deflected in the same sense. Because dynamic stress change is superposed on initial, pre-stress shear traction directions, and these differ between the two segments, the final curved slip paths for two differently oriented segments will achieve different final directions of slip, though the sense of curvature of these slip paths will typically be the same if the differences in segment dips are not great (Fig. 2E and F). A minority of the nonplanar faults modelled by these authors, those with strongly restraining or releasing segments, yielded an opposite ("abnormal") sense of slip-path convexity on the secondary fault relative to the main one. For this reason, Aoki et al. (2023) suggest that in the field one should focus on geometrically simple, more planar parts of faults to infer propagation directions from inscribed patterns of slickenline curvature. Finally, Macklin et al. (2021) modelled planar fault ruptures in elastic half-spaces that feature variable seismic velocities. In these layered models, the predicted senses of slickenline curvature relative to fault type and propagation direction do not differ from those of the homogeneous models (e.g., Fig. 2A–D). Some model configurations that

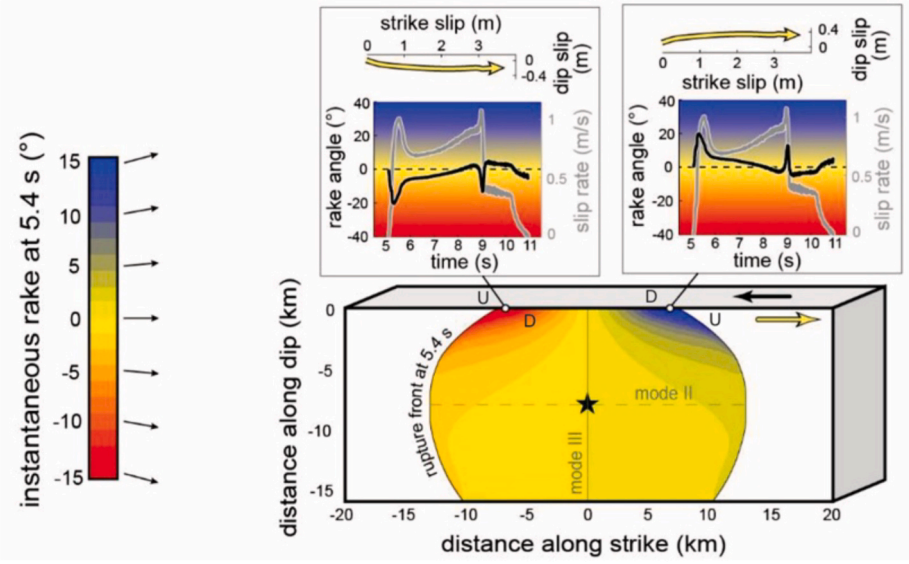


**Fig. 1.** Fault plane view of dynamic rupture simulation results for case of a vertical strike-slip fault (sinistral). Colors describe the instantaneous slip direction of the near side of the fault (not shown) relative to the far side at 5.4 s after rupture. Panels above the fault plane show the history of slip-vector rake angle (black curve, left hand ordinate) and slip-rate (grey curve, right-hand ordinate) at each end of the rupture. The yellow arrows depict the corresponding slip paths (i.e., slickenline trajectories) on the fault plane. For reference, the orientation of a mode II rupture boundary is shown as dashed horizontal line, and a mode III one as solid vertical line. These orientation lines are drawn through the hypocentre (black star). Note how on both sides of the hypocenter, the rupture front at 5.4 s is mixed-mode (II-III) at the ground surface. The color bar on the left depicts the instantaneous rake angle of slip on the fault plane (red colors, near block moving down; blue colors, near block moving up). (For interpretation of the references to color in this figure legend, the reader is referred to the Web version of this article.)

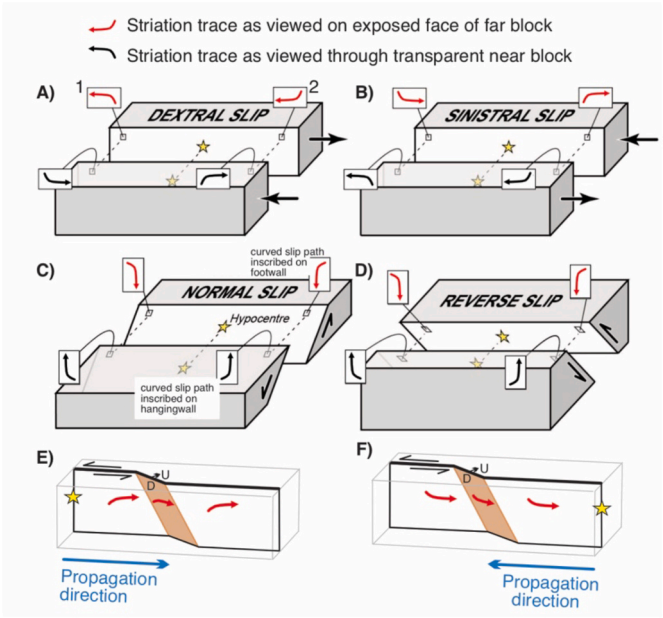


**Fig. 2.** Curved slickenline patterns expected to form during surface-rupturing earthquakes for different Andersonian fault types. Yellow star indicates location of earthquake hypocentre. Red curves depict slickenlines inscribed on the far fault lock as seen by a viewer who is looking face-on towards that block. The arrowhead indicates the youngest (last inscribed) part of the slip track. The black curves depict slickenlines inscribed on the near fault block where that block is transparent and the viewer is looking at the fault surface from behind. A) Dextral-strike slip fault; B) sinistral strike-slip fault; C) normal-slip fault; D) reverse slip fault. E) shows curved slickenlines on a contractional fault bend of a sinistral-slip fault where the rupture is propagating from left to right (compare to right-hand part of B); F) shows the same fault geometry as in E, but for a case where the rupture is propagating from right to left (compare to left-hand part of B). Note how the final orientations of slickenlines on the contractional bend in figures E) and F) are plunging in a way that indicates oblique-reverse motion (near block moving down relative to far block), whereas on the main fault the slip direction becomes strike-slip (horizontal). Despite the differences in the shape of slickenlines on the contractional bend relative to the main fault, the directions of their convexity are here the same, as they chiefly depend on the direction of rupture propagation. Figure modified from Kearse and Kaneko (2020). (For interpretation of the references to color in this figure legend, the reader is referred to the Web version of this article.)

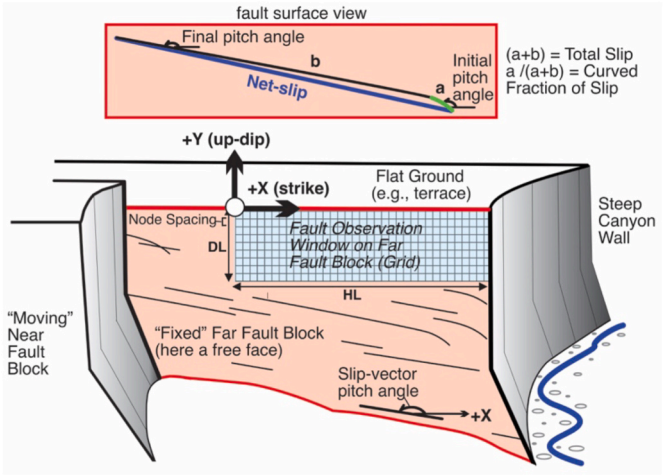


**Fig. 3.** Cartoon illustrating the fault plane reference system used in the program *Slicks*. The program considers a rectangular observation window of strike-parallel length, HL, and dip-parallel width, DL, that is attached to the "fixed" far block. In the observation window, a grid is constructed parallel to the x-y coordinate axes at a specified nodal spacing. The top of the observation window (bold red line) represents a flat ground surface on the pre-faulted landscape. The right-hand edge (bold black line) represents a vertical face, such as a steep canyon wall. Random asperities (not shown here) are seeded on the "moving" near block, which is displaced along a prescribed slip-path of some specified total length and shape. A direction of slip is specified by a slip-vector pitch angle. This angle may be constant or changing for a curved path (difference between initial and final pitch angles). The figure illustrates how a strike-slip rupture may exhume a free face where the fault offsets a steep gully or canyon wall. (For interpretation of the references to color in this figure legend, the reader is referred to the Web version of this article.)

feature a shallow (<1.5 km-deep) low-velocity zone, however, generate multiple rupture fronts. The corresponding slip-tracks for these models are locally more irregular in shape than for an idealized homogeneous case, and may feature larger total rake-angle deflections of up to 50–60° (Macklin et al., 2021).

## 3. Geometric modelling of curved slickenline patterns on scarps

Purely geometric and kinematic in its formulation, the program *Slicks* was written in MATLAB to simulate the shapes, lengths and topologies of populations of curved to straight slickenline tracks on fault surfaces. It considers a 2D rectangular patch of fault surface that, before slip, is seeded with randomly distributed asperities at a specified density. During a modelled earthquake, the fault is subject to a slip of predetermined direction, length, and curvature (if any). Asperities embedded in the "moving," near fault block inscribe slickenlines on the "fixed," far block. Each slickenline progressively lengthens as the slip accrues, but such growth may terminate if the asperity inscribing that striation is worn out or removed before the end of the slip path is reached. Such destructions are governed by a statistical "death" law for asperities (see below). Finally, as fault slip accumulates, neo-formed asperities may nucleate randomly on the fault plane according to a statistical "birth" law. Opposite any active asperity, be it original or neo-formed, slickenlines will continue to lengthen until that asperity either "dies" or the end of the prescribed total slip is reached, whichever comes first. By changing a set of input parameters (e.g., shape and length of the slip-path, original density of asperities, mean rates of asperity "death" vs. "birth," and the variability in these two rates) the program can simulate a diversity of slickenline patterns. These patterns differ from one another in the intersecting topologies of their slickenlines and the statistical length distributions of the final population of striae.

The reference system used by *Slicks* is shown in Fig. 3, and the input parameters needed for a model run are described in Table 1. The program considers a rectangular region (observation window) of strike-parallel length, HL, and dip-parallel width, DL, that is attached to the "fixed" far block. In the observation window, a grid is constructed parallel to the x-y coordinate axes at a specified nodal spacing. The top of the observation window (bold red line) represents a flat ground surface, such as a terrace, that lies on the pre-faulting landscape. The right-hand edge of the window (bold black line) represents a vertical face, such as a steep canyon wall cut by the fault. Random asperities (not shown in Fig. 3) are seeded on the near block, and these are later displaced along a slip-path of prescribed total length and shape. A direction of slip on a slip path is specified by its pitch (angle from the horizontal measured in the fault plane). For a straight slip trajectory, this angle is constant. For a curved slip-path, it varies. In this latter case, the slip-path is divided into two segments. The earlier-formed segment, envisioned as forming at the onset of slip in the rupture process zone, is curved. Its length is set to be a specified fraction of the total slip magnitude. In the program, the curved shape and convexity of this segment can be chosen to mimic the pattern of slip variation to be expected in the process zone of a rupture of a particular slip mechanism and propagation direction (Fig. 2). Over this early-formed, curved interval, the slip vector pitch angle (in degrees) is made to vary smoothly and linearly between a prescribed initial and final angle. The second, younger slip segment is linear and

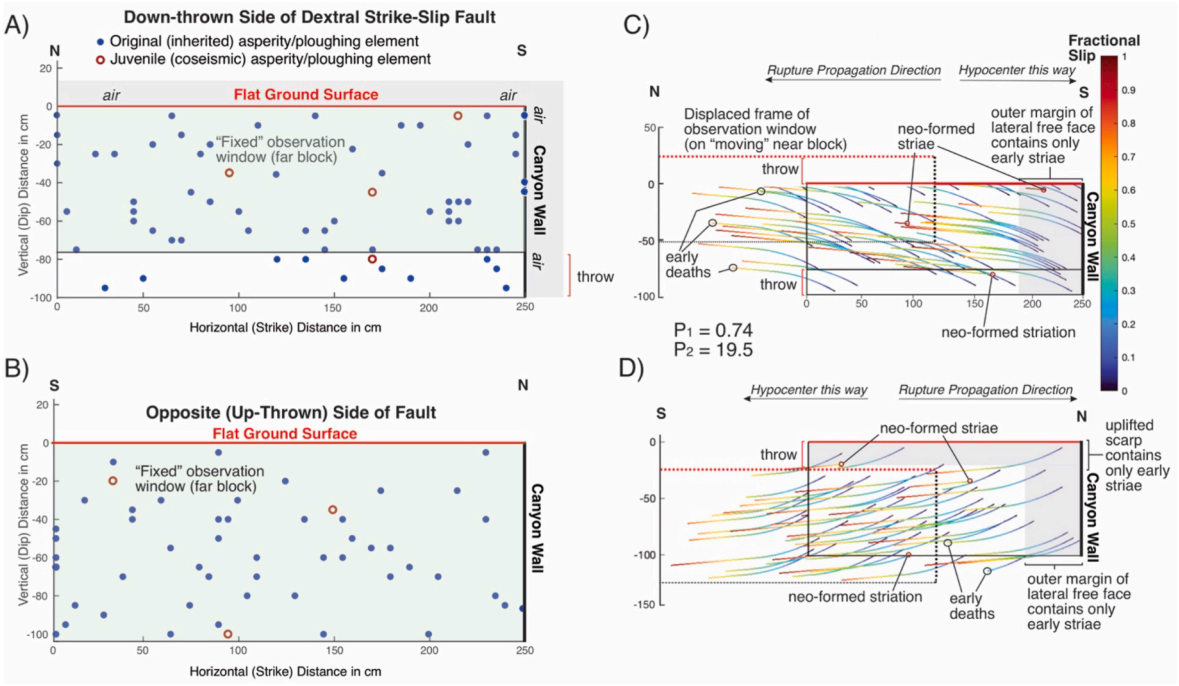


**Fig. 4.** Graphical output from *Slicks* for the default strike-slip model. The input parameters are listed in Table 1. A) Fault plane view looking towards the down-thrown eastern fault block showing pre-slip locations of original asperities (blue dots) and future neo-formed asperities (open red circles). These locations are projected from the "moving" near block onto the "fixed" far block. Note that the observation window is narrower in the dip direction than the field of asperities. This is done deliberately to prevent an artificial edge affect (deficiency of slickenlines) at the base of the model. Because the throw component can carry asperities and their slickenlines into the window from below, an extra width of asperities must be seeded below the window for that window to show a representative (i.e., untruncated) pattern of slickenlines at the end of the slip (see Fig. 4C). B) Fault plane view looking towards the upthrown western fault block showing pre-slip locations of original and future neo-formed asperities (same symbols as above). As expected, the particular locations and number of the randomly assigned asperities on each block is different. C) Slickenline tracks generated by slip of the asperities depicted in part A. The slickenlines are color coded according to the time (fraction of total slip path) of their inscription. Labels identify where some slickenlines terminated before the end of slip because of their "early death," and also where neo-formed tracks nucleated after slip had begun. Also identified (grey shading) is the area where early, curved portions of slickenlines are best preserved (not overprinted), which is on the leading edge of the lateral free face near the offset canyon wall. The convex-upward shape of the slickenlines in this view reflects rupture propagation from the right (South). D) Fault plane view showing slickenline tracks generated by slip of the asperities depicted in part B. The convex-downward shape of the slickenlines in this view reflects rupture propagation from the left (South). Note that In addition to free faces near offset canyon walls, the early, curved portions of slickenlines are well preserved along uplifted scarps displacing an originally flat ground surface. See text for definition of $P_1$ and $P_2$. (For interpretation of the references to color in this figure legend, the reader is referred to the Web version of this article.)

accommodates the balance of the total fault slip magnitude at the final pitch angle. Along the prescribed slip trajectory, slip is accumulated iteratively in small linear segments at a specified fault-slip step size (typically chosen to be smaller than the grid spacing) until the total slip is achieved.

Asperities are considered to be point features on the "moving" near block, and their initial density (number per $m^2$) on the fault plane is prescribed in the input file. Based on this density, the program randomly populates the grid with a corresponding number of asperities. These points will move according to the prescribed the slip path, each inscribing a slickenline on the "fixed" block. As slip accrues, the position and shape and length of each slickenline is logged by the program. At each small incremental slip-step, the current survival status of each asperity is reassessed by taking a Monte Carlo sample of the prescribed "death law." The law is assumed to be a normal distribution defined by the mean asperity "death age" (longevity specified as a mean slip distance before erosion or removal) together with a standard deviation for that distribution of survival ages. Finally, during the slip path, neo-formed asperities are introduced randomly into the grid at an average frequency that is governed by a "birth law." This law determines the density of new asperities (number per $m^2$ of fault surface) that form per meter of accumulated fault slip. For each model run, a nucleation rate that pertains to the specified total slip distance is sampled from a normal distribution having a specified mean value and standard deviation (Table 1). The corresponding number of nucleations are introduced randomly in time during the slip-path (i.e., as a Poissonian process).

## 4. Strike-slip example

Fig. 4 shows the results of a model that simulates the pattern of curved slickenlines resulting from a dominantly strike-slip rupture slipping 1.3 m dextrally and 0.24m vertically (1.35 m of total slip) during a surface-rupturing earthquake that propagated into the site from the south. This example illustrates several general points pertaining to curved slickenline patterns and their interpretation, and we refer to it as the default model. Fig. 4A plots the pre-slip location of a random set of original asperities in the near (western) block where they abutted against the far (eastern) fault block, which will be slightly downthrown. Fig. 4B, looking the other direction, depicts a different random set of asperities in the eastern block where they abutted against the western fault block. The fault slip-path parameters used in this model (Table 1) were chosen to mimic some aspects of the 2016 earthquake on the Kekerengu Fault, which propagated to the NE, generated curved slickenlines that were convex-up as observed looking onto the eastern block, and slipped obliquely with an up-to-the-NW sense of net throw (Fig. 4C). Even though the actual dextral-slip on the Kekerengu Fault in 2016 was typically 7–10 m, for the default model we chose a smaller value of 1.35 m because this smaller slip length allows the main features of the entire slickenline pattern to be depicted in an observation window that is 2.5 m wide rather than >10 m wide (HL in Table 1), thus enhancing the

**Table 1**
Explanation of input variables used in the program *Slicks*.

| Input Variable | Value in Default Run ( Fig. 4) | Explanation |
|---|---|---|
| HL | 255 | Horizontal length (strike distance) of fault plane observation window (in cm) |
| DL | 105 | Dip-direction-parallel length (depth) of fault plane observation window (in cm) |
| Spacing | 5 | Node spacing on grid (in cm) |
| Asp_Density | 24 | Average initial density of asperities on the "moving" near fault block (number per m2 of fault surface) |
| Total_Slip | 135 | Total (cumulative) distance of fault slip during the model run (in cm) |
| Slip_Increment | 0.375 | Distance of a single fault-slip step (in cm) |
| Curv_Frac | 0.44 | Fraction of fault-slip path that is curved (starts at track initiation, number between 0 and 1) |
| Initial_Angle | 150 | Rake of the initial slip-vector increment (degrees anticlockwise from +x direction; motion of near block relative to "fixed" far block) |
| End_Curve_Angle | 175 | Rake of the last the slip-vector increment on curved part of slip path (also of subsequent straight path, same conventions as above) |
| Mean_Death_Age | 100 | Mean slip distance (in cm) that an asperity survives before it is removed from fault contact (part of assumed normal distribution) |
| DAcov | 0.30 | Coefficient of standard deviation of survived slip distances (ratio of standard deviation of distribution to variable, Mean_Death_Age) |
| k | 1.00 | Birth-rate factor: Average density (number per m2) of neo-formed asperities per meter of fault slip (assumed normal distribution) |
| cov | 0.25 | Coefficient of standard deviation of distribution of neo-asperity densities (ratio of standard deviation of distribution to variable, k) |

P1 = Mean_Death_Age/Total_Slip = 0.74 in Default Run.
P2 = Asp_Density/(k*Total_Slip/100) = 19.5 in Default Run.

relative size and detail of individual tracks plotted in a window that has a fixed size on the printed page. In the default model, we input a mean asperity slip distance (coding parameter called Mean_Death_Age in Table 1) that is similar to the total slip magnitude (Total_Slip). This choice reduced the number of asperity "deaths" during the run, thus promoting inscription of long slickenline tracks that record the full slip history. Long, complete tracks were further encouraged by inputting a small asperity birth rate factor (parameter, k in Table 1). This latter choice suppressed the formation later-forming, short slickenline tracks recording only a fraction of the slip-path.

Fig. 4C plots the modelled population of curved slickenlines generated by movement of the asperities depicted in Fig. 4A. The color coding used for the slickenlines specifies the fractional "timing" of inscription of each point on a striation trace relative to the total slip path. Slickenlines that are not drawn with a dark red color at their downstream ends were inscribed by asperities that "died" (were removed) before attaining the end of the simulated earthquake slip. Conversely, tracks that do not initiate with a dark blue color record asperities that were "born" (nucleated) coseismically during the slip (several examples of both of these cases are labelled in Fig. 4C and D).

The model illustrates that for a single earthquake, the direction of convexity of slickenline tracks flips depending on which fault block is being observed. Fig. 4D shows slickenline traces for the same slip model as in Fig. 4C but as viewed looking in the opposite direction. In case 4C (looking east), the observation window is attached to the downthrown block, and the rupture is propagating from right to left. In case 4D (looking west), it is attached to the upthrown block and rupture is propagating from left to right. A key point to be made from this comparison is that the locally observed sense of slickenline curvature (e.g., convex-up or convex-down) depends not only on the rupture propagation direction, but also on the observer's direction of view. Thus without first specifying the viewer's perspective, the direction of rupture propagation (in this case towards the north) cannot be inferred simply by citing the locally observed sense of slickenline convexity (see also Fig. 2).

Fig. 4C and D reveal that curved slickenline traces intersect one another, potentially multiple times along a given track. These are not the result of multiple earthquake events but rather of the changing direction of slip during a single event. Earlier-formed track segments, which are curved, are overprinted by later-formed ones, which may be straight. For a given asperity density, the frequency of such intersections will increase as the curvature of the slip-path increases and the total magnitude of slip (track length) increases. Note that intersections produce apparent "kinks" between adjacent track segments that might be misconstrued as an abrupt change in slip direction on a single, continuous track rather than the overriding of an early-formed part of one track by a later-formed part of another. Importantly, if the former misinterpretation is used to assign a local sense of curvature convexity, the wrong direction of rupture propagation might be inferred for the site (e.g., in Fig. 4D gradational curvature of individual slickenlines is convex-down, whereas the abrupt convexity defined by two intersecting tracks is sometimes convex-up).

The model also illustrates the role of edge effects on the expression of curved slickenline patterns. Asperities originally located near the left edge of the observation window (simulated outcrop face) in the default model are dextrally displaced to final positions outside of the window. In other words, slickenlines at the margins of an outcrop generally reveal only partial track lengths (the remainder being concealed beneath the other fault block). Another edge is the topographic surface. If a strike-slip rupture offsets a deeply incised canyon or gully, a free face may form as a result of the lateral offset of the canyon wall (Fig. 3). As one fault block is shunted away, its asperities will incise slickenlines onto the opposite fault surface, and these tracks will be immediately exposed on the resulting free face. Because the removed block has been replaced by air, no further asperities can rake across that face; thus any early-formed, curved tracks inscribed on the face cannot be intersected or overprinted during later parts of the earthquake slip. Adjacent to the canyon wall, the free face margins are especially likely to preserve curved slickenlines because this part of the scarp was exhumed at the time of slip initiation (Fig. 4C and D). Similarly, where a rupture has slipped in part vertically, early-formed, curved slickenlines will be preferentially preserved along the top of an uplifted scarp on flat ground (Fig. 4D).

## 5. Dip-slip example

Fig. 5 presents slickenline plots resulting from a dip-slip version of the default model; specifically a simulated normal-slip earthquake with a rupture propagating into a site from the north. The input parameters for this model are the same as those in the strike-slip model, except that the slip direction (hangingwall relative to footwall) is now mostly down-dip. The expected sense of early slickenline curvature is convex-to-the-north on the footwall block, and concave-to-the-north on the hanging-wall block (see Fig. 2). Because the footwall block self-exhumes a strip of fault surface during the earthquake, the slickenlines exposed near the top of this uplifted scarp were inscribed at the beginning of the earthquake; thus they are curved and were not overridden by later-formed, straight striation segments. By contrast, the hangingwall of the fault is remains buried during the slip, and its curved slickenline segments are prone to overprinting by later straight ones.

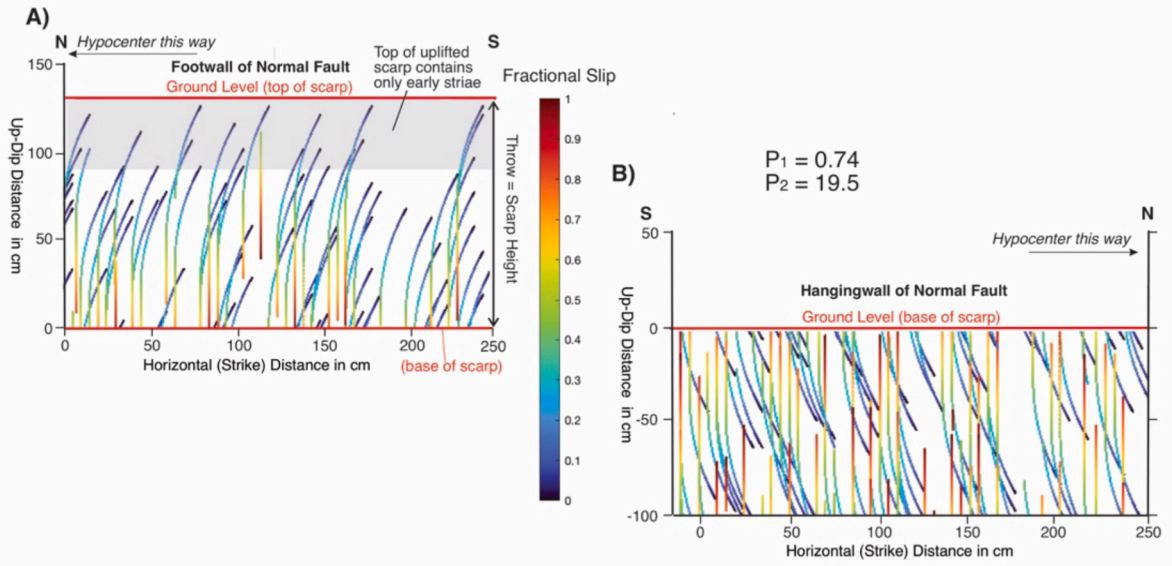


**Fig. 5.** Graphical output from *Slicks* for a normal dip-slip model (same default input parameters as listed in Table 1, but with slip-path rotated to down-dip). A) Slickenlines inscribed on the footwall for a case where hypocentre is to the left (rupture propagates from the north). Light-grey shading identifies a region at the top of the scarp on the uplifted block where the curved, older parts of slickenlines are best preserved (least overprinted). B) Slickenlines inscribed on the hangingwall for a case where hypocentre is to the right (rupture propagates from the north). Because this block is downthrown, no part of the fault surface is exhumed on it during the slip, thus intersecting (overprinted) slickenlines are equally frequent on all parts of the fault surface.

## 6. Variable patterns and length distributions of slickenlines

### 6.1. Generating variable slickenline patterns from a single slip-path

During a model run, *Slicks* tabulates the length and shape of each growing slickenline. Four temporal-geometrical categories of striae can be recognized: 1) those that initiate at the beginning of the earthquake and that lengthen continuously throughout the entire slip path; 2) those that initiate at the start of the earthquake but that terminate "early" because the corresponding asperity is removed before full slip is achieved; 3) those that initiate at some point during the earthquake (not at the beginning) and that persist throughout the rest of the slip; and 4) those that initiate at some point during the earthquake (not at the beginning) and that do not survive until the end of the slip because its inscribing asperity is removed before full slip is achieved. In the program, the relative abundances of these track types are controlled by the relative values of the asperity "death-rate" and "birth-rate." These rates are determined by the mean slip distance (longevity) that an asperity survives before its death or removal (parameter, Mean_Death_Age in Table 1), the average density of newly formed asperities that form per meter of fault slip ("birth-rate" factor, k, in Table 1), and the specified coefficients of standard deviation for these two rates (DAcov and cov, Table 1). With *Slicks*, one can easily forward-model slickenline patterns and length distributions as a function of the values chosen for these variables.

To visualise the development of varying slickenline patterns, it is convenient to define two dimensionless parameters. The first $P_1$:

$P_1$ = Mean Asperity Slip Distance (in meters) / Total-Slip (in meters)(1)

$P_1$ is the fractional distance over which an average asperity maintains contact with the fault surface relative to the total slip of the earthquake. It is a measure of mean asperity durability normalized by the slip distance (Table 1). Where this durability parameter is close to 1 or greater, many slickenline tracks are likely to achieve a final length that is equal to the total slip. Where $P_1$ is smaller than 1, most slickenline tracks will be shorter than the total slip. The second parameter, $P_2$:

$P_2$ = Density of Original Asperities / Density of Neo-Formed Asperities (2)

$P_2$ is the ratio between the average density of original asperities existing prior to the onset of slip (number of per $m^2$ of fault surface) and the average density of neo-formed asperities that are introduced onto the fault surface coseismically during the slip. The denominator is the product of 1) the average density of new asperities generated per meter of fault slip; and 2) the total fault slip in meters (Table 1). A high value of $P_2$ thus describes a case where few new asperities nucleate during the slip, whereas a low value of $P_2$ describes a case where newly generated, juvenile asperities are dominant.

### 6.2. Variable slickenline topologies

Fig. 6 shows how diverse types of slickenline topologies can be generated from the same slip-path (in this case, the default one) by independently varying $P_1$ and $P_2$, while holding all other input parameters the same as those in the default model of Fig. 4 (see Table 1). Fig. 6A shows a fault map plotting randomly generated asperity locations for a model run in which $P_2 = 1.5$ (slightly more original asperities than neo-formed ones). Fig. 6B shows a map of randomly generated asperity locations for a model run in which $P_2 = 0$ (only neo-formed asperities are present). In the first scenario ($P_2 = 1.5$, left-hand column of Fig. 6), C, 6E, and 6G show the effect of increasing $P_1$ (asperity longevity parameter) from 0.25 to 0.5 to 0.75, respectively, in a case where original asperities are abundant. In the second scenario ($P_2 = 0$, right-hand column of Fig. 6), D, 6F, and 6H show the effect of varying the relative asperity durability ($P_1$) for a case where only neo-formed asperities are present. The variation between these plots allow us to make some general statements about slickenline topologies: 1) Both the mean length of slickenline tracks and the density of their intersections increase as asperity durability increases; 2) curved tracks can only be inscribed by original or early-formed asperities, and are most abundant where original asperities are numerous; 3) track intersections require the presence of curved tracks (see point 2, above); and 4) completely straight tracks can only be inscribed by neo-formed asperities.

### 6.3. Slickenline track-length distributions

The competing effects of asperity durability ($P_1$) versus the ratio of

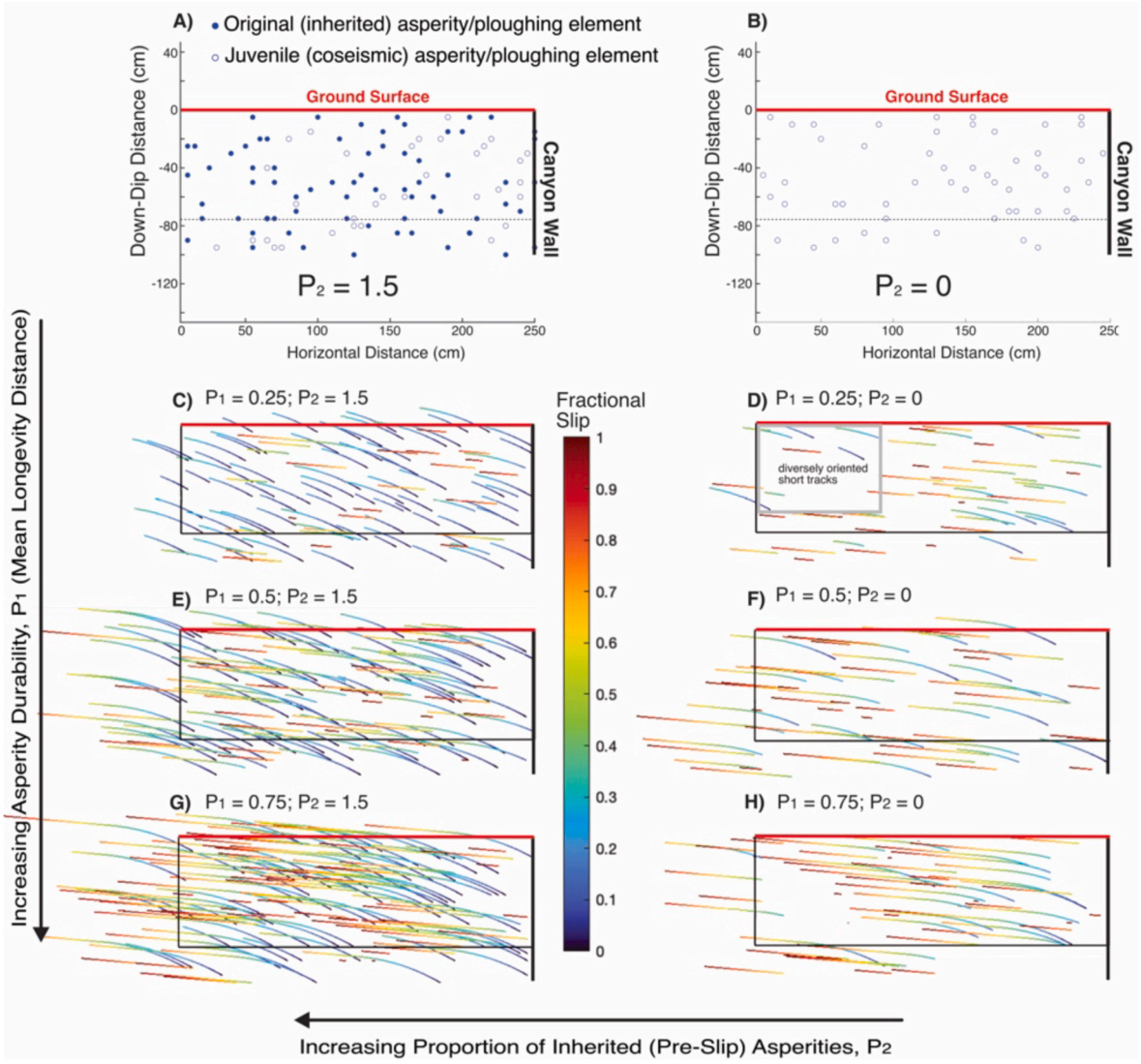


**Fig. 6.** Outputs from *Slicks* illustrating how slickenline topologies vary as a function of the dimensionless parameters $P_1$ and $P_2$. $P_1$ (ratio of mean asperity slip distance to total-slip magnitude) increases down the page. $P_2$ (ratio of inherited, pre-slip asperities to neo-formed, syn-slip ones) increases from right to left. All models use mostly the same input values as those in the default strike-slip model shown in Fig. 4, except they vary $P_1$ and $P_2$. A) Fault plane view showing pre-slip locations of a set of original asperities (blue dots) and future neo-formed asperities (open, light blue circles) for a model run in which the numbers of original and neo-formed asperities are set to be about equally abundant ($P_2 = 1.5$). B) View of asperity locations for a case where all these are neo-formed, and none existed prior to slip ($P_2 = 0$). C) Slip window plot for asperity set in part A with $P_1 = 0.25$. D) Slip window plot for asperity set in part B, again with $P_1 = 0.25$. The small box labelled "diversely oriented short tracks" embraces a section of fault surface that contains only short tracks. Each is straight or at most only slightly curved, and none intersect; yet the diversity of their rakes preserves evidence for a longer slip path that was curved. For each of the other model runs (E, F, G, and H), new asperity location sets must be randomly generated afresh. Those in the left-hand column are all based on $P_2 = 1.5$ (subequal frequency of the two asperity types, as in part A), and those in the right-hand column on $P_2 = 0$ (only neo-formed asperities, as in part B). See text for additional description of $P_1$ and $P_2$. (For interpretation of the references to color in this figure legend, the reader is referred to the Web version of this article.)

inherited/neo-formed asperities($P_2$) on slickenline lengths is illustrated for a range of arbitrary values in Fig. 7. For generality, we normalize slickenline lengths by the total-slip magnitude. The x-axis of the main plot represents the asperity durability (longevity) parameter $P_1$. As $P_1$ increases, the mean normalized track length (plotted on the y-axis) always increases (see colored curves in Fig. 7, with each curve representing a different value of $P_2$). Where $P_1$ approaches 1.0, many tracks will survive through the entire slip-path and their length will be equal to the total slip distance (= normalized track length of 1.0). If $P_1$ exceeds 1.0, then a majority of tracks will achieve this maximum length (unless $P_2$ is close to zero).

Track lengths are also affected by the relative timing of asperity nucleation, $P_2$. For constant asperity durability, $P_1$, the greater the fraction of neo-formed asperities (case of low $P_2$), the shorter the average track length will be. This is because neo-formed asperities can only inscribe a fractional slip path—and potentially only a very short one. By contrast, asperities that have been present from the onset of slip (most abundant in case of high $P_2$) have the potential to inscribe a long or even full-length track (if they are durable enough). Note that the shape of the curves also change with $P_2$. In a case where there are only neo-formed asperities and no original asperities (i.e., an initially smooth fault, $P_2 = 0$, the blue curve), then as the durability $P_1$ increases the mean normalized track length approaches an asymptotic maximum value of 0.5. This is because random asperity nucleation causes an approximately equal number of tracks to initiate before and after the mid-point of the slip-path. For this reason, even if the asperities are very durable and there are no track "deaths" ($P_1 \gg 1.0$), half of the tracks will have a mean normalized length greater than 0.5, and half smaller than

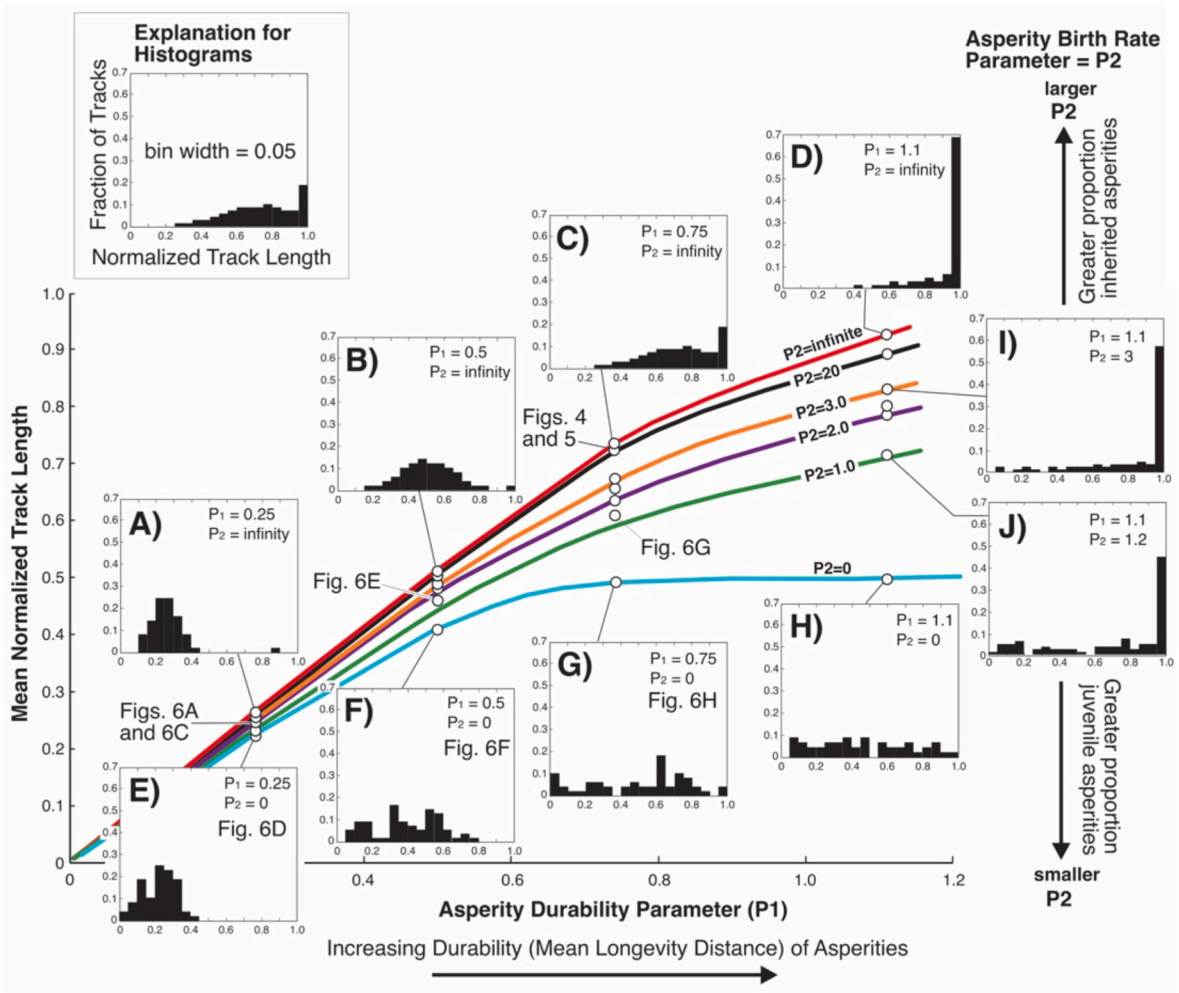


**Fig. 7.** Plot of mean normalized slickenline length vs. the asperity longevity parameter ($P_1$) based on 24 different runs of the program *Slicks* using mostly the same input parameters as those in the default strike-slip model of Fig. 4, but employing a range of different $P_1$ and $P_2$ values. The colored contour lines denote $P_2$ values (ratio of densities of original to neo-formed asperities) between 0 (neo-formed asperities only) and infinity (inherited asperities only). For selected model runs, histograms plot normalized track lengths (ratio of track length to total slip magnitude) vs. the fraction of tracks. The bin interval is 0.05. See text for additional description of $P_1$ and $P_2$.

0.5.

The selected histograms included on Fig. 7 show how track length distributions vary as a function of $P_1$ and $P_2$. Parts A) through D) present a series with increasing $P_1$ (asperity durability). The series pertains to an end-member case where all asperities are inherited ($P_2$ = infinity). An obvious feature of this series is the appearance of a mode of maximum-length tracks as the asperity durability $P_1$ approaches or exceeds 1.0. This aspect of the distribution reflects the fact that a) individual striae cannot grow longer than the total-slip of the earthquake that formed them; and b) the greater the asperity durability ($P_1$), the greater the number of such maximum-length slickenlines in a population. By contrast, where the asperity durability is weak ($P_1 \ll 1.0$), the track length distributions are characteristically symmetrical about a mean value equal to the durability ratio, $P_1$. This is because *Slicks* assumes a normal distribution of survival distances for its asperity "death law." If we had invoked a larger standard deviation for this law (i.e., greater than 30% of the mean survival distance, Table 1), then the normal distributions in Fig. 7A and B would be correspondingly broader, but the basic shapes and symmetries would remain the same. Parts E) through H) present a series with increasing asperity durability, $P_1$, for the extreme case where the fault begins as a perfectly smooth surface ($P_2$ = 0). In this scenario, all the asperities are neo-formed ones. Because each asperity nucleates randomly at a different point in the slip-path, slickenline lengths are more broadly and irregularly distributed than for the first-mentioned series. Lastly, Fig. 7D, I, 7J, and 7H represent a series in which asperities (once formed) are durable and long-lived ($P_1$ = 1.1), but with $P_2$ decreasing down the page from infinity (100% inherited asperities, Fig. 7D) to zero (100% juvenile ones, Fig. 7H). In the last case, it is unlikely that any neo-formed asperities will randomly nucleate at "time zero." For this reason, even though the inscribers are durable, few slickenlines will achieve the maximum possible length, and the plot therefore shows no mode corresponding to a normalized track length of 1.0 (Fig. 7H).

## 7. Natural slickenlines on the active Kekerengu and Alpine Faults, New Zealand

The Mw 7.8 Kaikōura Earthquake nucleated at a depth of ~14 km within the continental crust of the northeastern South Island on November 14, 2016, propagating unilaterally in a northeast direction for ~180 km during approximately 120 s of ground motion (Kaiser et al., 2017; Ando and Kaneko, 2018). The earthquake ruptured at least 20 faults that have variable attitudes, slip magnitudes, and slip rates, forming a complex network of locally intersecting ruptures in the Pacific-Australian plate boundary zone (Litchfield et al., 2018; Nicol et al., 2023). Focal mechanisms for the earthquake mainshock indicate

that it accommodated a combination of reverse and dextral-slip faulting (Kaiser et al., 2017).

The greatest moment release (Cesca et al., 2017; Holden et al., 2017) and largest slip at the ground surface (Kearse et al., 2018; Litchfield et al., 2018) took place on the Kekerengu Fault in the NE part of the rupture zone (Fig. 8A). Along a ~10 km-long section of that NE-striking fault, which mostly dips to the NW at 65–80°, many scarps were formed in bedrock or packed, cohesive gravels by slip during the earthquake. The dextral-slip was commonly 8–10 m (maximum of ~11 m); and the dip-slip was typically 1–2 m in an up-to-the NW (reverse) sense. Where the fault cuts across deeply incised stream canyons in solid rock, these gullies were laterally displaced to expose free faces (Fig. 3). Because the fault dips NW, the offset topography on that side of the fault (the hangingwall) was prone to gravitational collapse either during or soon after the earthquake, whereas the SE (footwall) side was stable. The free faces are remarkably smooth and planar exposures of the coseismically slipping fault surface. In some cases these scarps were up to 7 m long parallel to strike and 1–2 m wide parallel to dip (e.g., Fig. 8B and C). The faces were inscribed by abundant slickenlines, many of them curved.

The slickenlines decorate a 1-2 cm-thick layer of soft fault gouge smeared on the bedrock that quickly desiccated after the earthquake and fell away within a few weeks of that event (Kearse, 2018; Kearse et al., 2018, 2019). Most striae had a spacing and relief that was at the mm to cm scale, although some larger "corrugations" up to several decimetres wide were locally observed (Fig. 8B). We interpret all of these striae as wear grooves, recording the passage of small asperities or ploughing objects that indented the gouge as they slipped past it. Such abrasive marks have been variably termed wear grooves, gouging-grain grooves, tool marks, prod marks, prod grooves, or moulded grain grooves (Means, 1987; Petit, 1987; Doblas, 1998; Tjia, 2014).

Kearse et al. (2018) were part of a response team deployed to evaluate and map the ruptures immediately after the 2016 earthquake. Due to time limitations, they were unable to measure many individual track lengths during their field work. Despite this limitation, important observations were made. At one locality, a set of contiguous tracks were observed to be ~6 m long (Fig. 8B). At all the other localities, individual tracks were <1.5 m long with the majority being <50 cm long. Curved slickenline tracks were observed on 10 of the 24 free faces examined (e.g., Fig. 8C and D). With two exceptions (both near local restraining bends), the sense of track convexity was upward where the observer was looking onto the SE block, and downwards where looking onto the NW block. This predominant sense of curvature was attributed by Kearse et al. (2019) to dynamic stress variation in the cohesive zone of a rupture that was propagating from the SW to the NE. Individual curved track segments had total deflections varying between 15 and 46° and occupied a track distance up to several tens of centimetres in length. This curved segment distance corresponds to <10% of the total slip. Some curved tracks were seen to transition downstream into a linear trajectory that pitched 5–15° to the SW (Fig. 8C and D). Such transitions record a coseismic change in slip direction towards subparallelism with the finite slip vector as defined by the offset of nearby fences or landforms. Finally, the linear segments of these partly curved tracks have the same orientation as the more abundant short, straight tracks that decorate the scarps.

As predicted by our models (e.g, Fig. 4A and B), slickenline tracks on 2016 scarps of the Kekerengu Fault locally intersected one another with older, more steeply pitching segments being overridden by younger, less steeply pitching ones (Fig. 8E and F). On scarps developed on nearly flat ground, curved tracks were found near the ground surface on the upthrown block (compare Fig. 4D—in particular, the upper grey-shaded region of scarp—with Fig. 8B). Where scarps developed on free faces chiefly as a result of strike-slip, the curved slickenline tracks were most common adjacent to the offset canyon wall (c.f., grey-shaded region on Fig. 4C on right-hand side of scarp to Fig. 8C). In addition, Kearse (2018) and Kearse et al. (2018) observed that the pitch of the total slip-vectors (up to 10 m long) for the earthquake as measured from 3D surveying of displaced linear landforms and cultural features were commonly more shallowly plunging than individual curved or short (several 10's of cm-long) slickenline striae observed on scarps adjacent to those landforms. Such discordance between incremental slip directions (slickenlines) and the total slip vector (offset landforms) provides further evidence for an overall curved slip path (e.g., Figs. 2, 4C and 4D. This relationship was interpreted from the literature for several historic surface ruptures by Kearse and Koneko (2020; see their Fig. 9). On 2016 earthquake scarps of the Kekerengu Fault, curved striation segments were no longer than ~10% of the total slip distance, thus it is not surprising that most striae imprinted into the record were both straight and shallowly pitching because this direction of slip was by far dominant.

Slickenlines on the Kekerengu Fault provided some evidence of individual ploughing elements being destroyed or removed. While most tracks terminated abruptly, suggesting a sudden abrasion, spalling or other mode of removal of the asperity from fault contact, others appeared to gradually shallow and widen towards the termination point (white circle, Fig. 8D). The latter relationship may record progressive abrasional removal of the asperity during slip. In a few cases, a discrete ploughing element was found embedded at the end of a terminating track (two white circles in Fig. 8F). These mm-sized clasts appear to have broken off one or the other wall of the fault, after which they adhered to the inscribing (non-observed) block. Eventually the clasts left the inscribing block to be accreted onto the observed block. This transfer terminated inscription of the track on that block. After this, it is possible that the same clast may have begun incising a new track on the opposing (non-observed) block. By this block-switching process, an asperity "death" on one block may coincide (spatially and temporally) with an asperity "birth" on the opposite one, all of it occasioned by a single rigid clast acting as a third body between the two slipping sides of the fault.

Natural outcrops along the southern Alpine Fault (Fig. 8A) expose slickenline tracks that were inscribed on the fault plane during surface-rupturing paleoearthquakes, including the last one in 1717 CE, which is inferred to have slipped dextrally by ~8 m and had an Mw of 8.1 ± 0.1 (Barth et al., 2024). At Hokuri Creek (Fig. 9A parts A-1 and A-2), curved tracks are common. Two deeply incised "clusters" of tracks are each up to 3.5 m long and (viewed from the SE) have similar convex-downward shapes that deflect through ~19 ± 2° of rake (Fig. 9, part A-3). Significantly, curvature is localized at the upstream ends of these tracks, transitioning to a longer and more representative, linear slip direction at their downstream ends, as predicted by dynamic rupture models (e.g., Fig. 1). The polarity of the curvature records northward rupture propagation at the site, though the age of the paleoearthquake is here unknown (Barth et al., 2024). At Martyr River (Fig. 9B, parts B-1 and B-2), the exposed fault plane faces the other way (viewed from the NW). Here convex-upward slickenlines (e.g., Fig. B-3) record a northward rupture propagation that Barth et al. (2024) attribute to the 1717 CE (last) paleoearthquake. Of special relevance are subhorizontal track segments overridden by NE-plunging ones (Fig. 9B, part B-4). We interpret this intersection between short, straight tracks to further reflect an overall convex-upward slip path (likely >5 m in total length). Using *Slicks*, one can forward-model the approximate striation pattern on this outcrop if the earthquake inherits few original asperities (early inscriber nuclei), and if the mean durability of the neo-formed ones is low to generate many short, straight tracks (Fig. 9C).

## 8. Discussion

### 8.1. Important field relationships for interpretation of curved slickenline patterns

It is important to acknowledge that for simplicity our modelling approach assumes that the fault is planar and that each successive earthquake completely overwrites any pre-existing striations. In reality, striations inherited from previous events may be preserved locally in the fault zone, especially in off-fault locations away from the principal slip

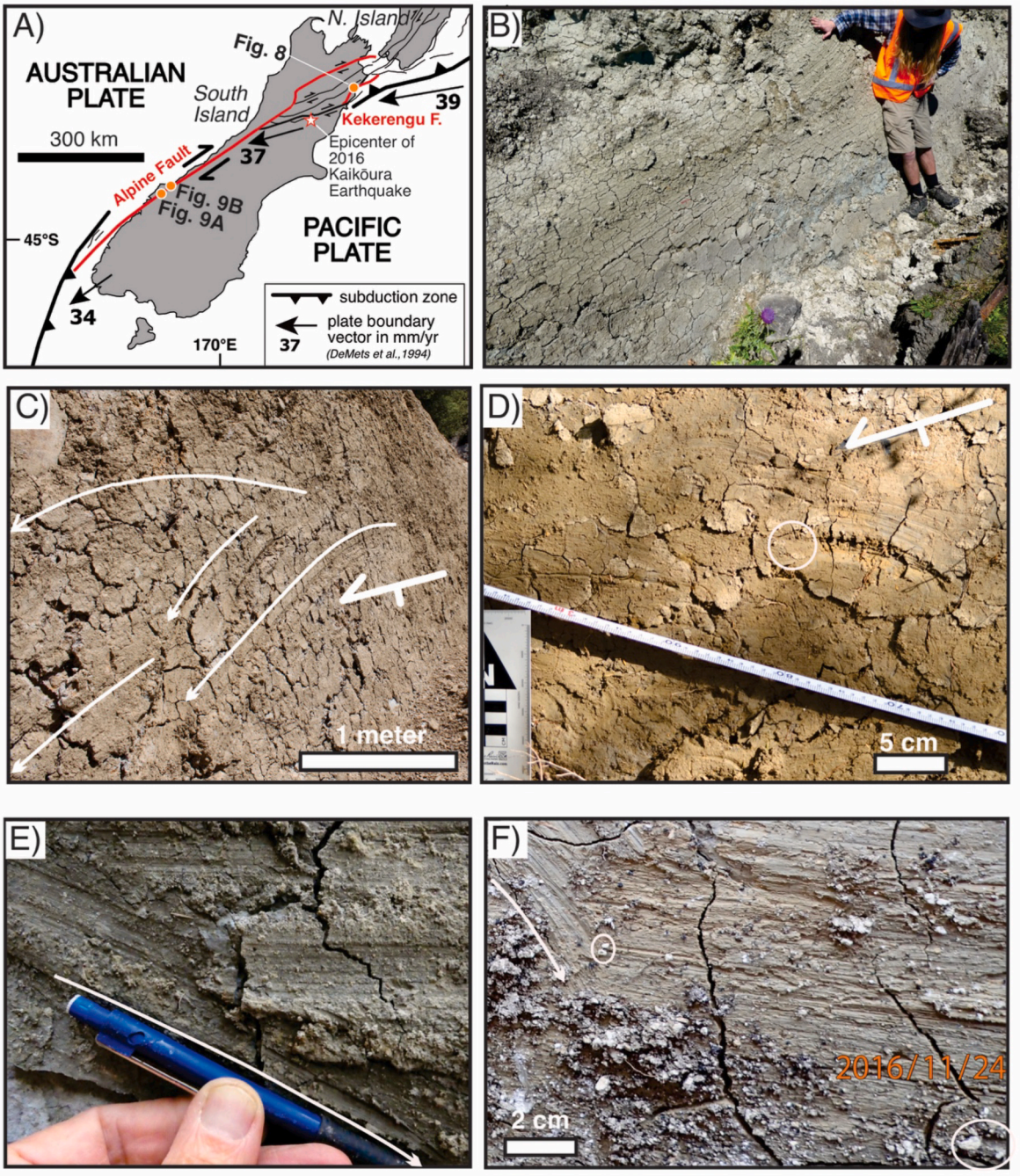


**Fig. 8.** A) Simplified map of a southern part of the New Zealand plate boundary zone showing active faults on which curved slickenlines were observed, including the Kekerengu Fault (scarps formed during the 2016 Kaikōura earthquake) and the Alpine Fault (slip surfaces inscribed during one or more paleo-earthquakes). B) Unusually long (>2 m-long) slickenline tracks on a steeply dipping scarp. Although motion was dominated by dextral-slip, the scarp at this site was exhumed by a subordinate component of normal dip-slip; this was highest during the early slip history (note curved striations below geologist's hand). The striations are inscribed in a 1-2 cm-thick layer of gouge that is smeared on hard bedrock on both sides. C) Steeply dipping lateral free face exposure, looking SE, of curved slickenline tracks. The canyon wall is in right-hand corner. White arrowheads point in the down-plunge direction. Upward convexity in this view is consistent with NE rupture propagation direction for a dextral-slip fault. D) Another subvertical lateral free face exposure of the Kekerengu Fault, looking SE. Note upward convexity of the curved, 10-20 cm-long tracks, consistent with NE-propagation. Note also the abrupt termination of many of the tracks at their ends, but with the white-circled track termination being diffuse. E) Straight slickenline tracks on a subvertical lateral free face override older track segments that are plunging and slightly convex-upward in shape. F) Another steep lateral free face exposure showing straight slickenline tracks overriding older track segments that are curved and plunging. As in E), the kink-like, downward convexity of the track intersection contrasts with the gradually curved, upward convexity of individual striae (see upper left-hand corner of the image). The latter sense of convexity is consistent with NE rupture propagation. White ovals identify "frozen-in" granule-sized clasts that have acted as ploughing elements in the gouge layer (DeMets et al., 1994).

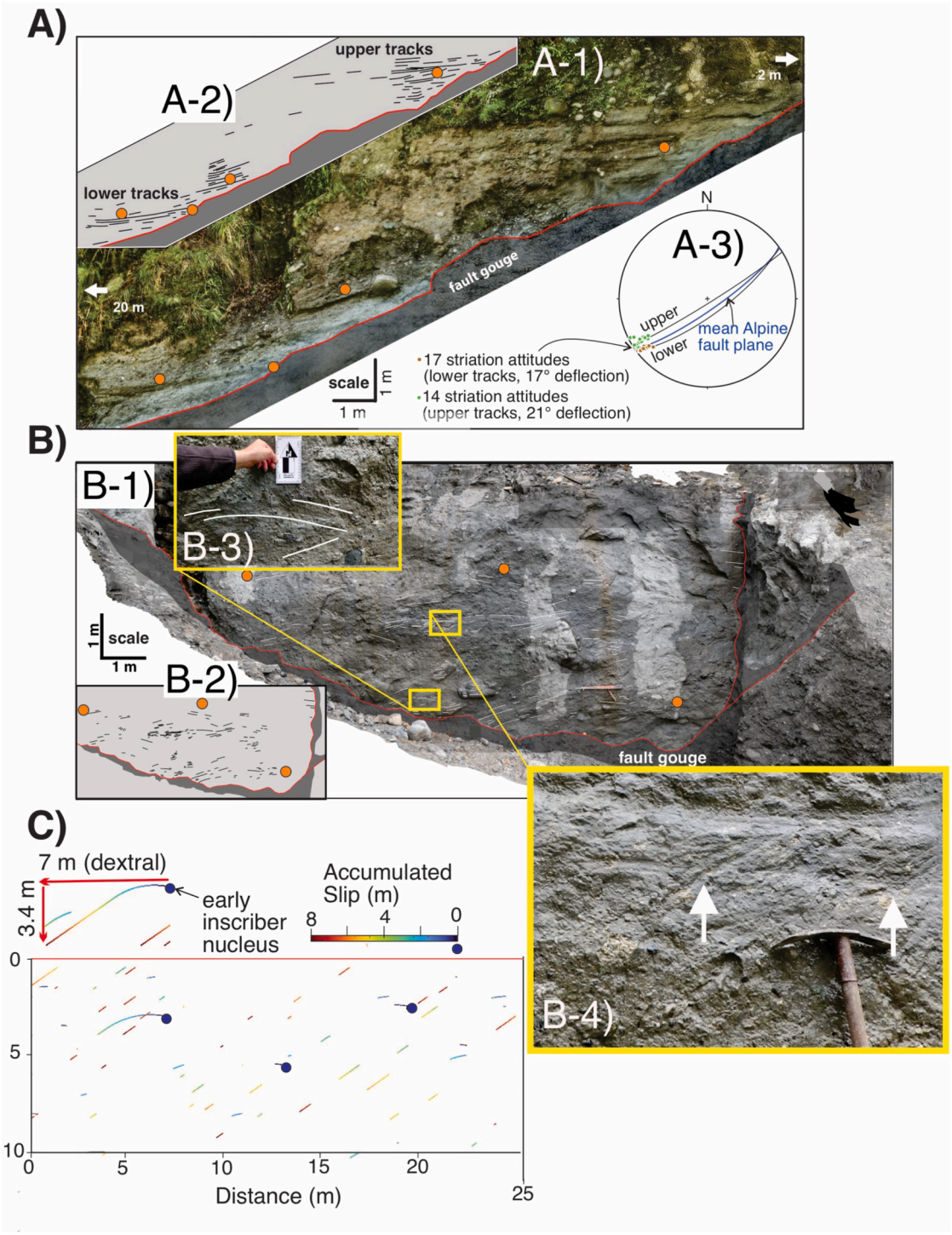


**Fig. 9.** Slickenlines preserved on naturally exposed, near-vertical slip surfaces on the Alpine Fault. For locations, see Fig. 8A. Locally, the area of track exposure was artificially enlarged with hand tools. The Structure-from-motion (SfM) model orthographic images of the outcrops (parts A-1 and B-1) and corresponding interpretive line drawings (at smaller scale) showing their preserved slickenline tracks (parts A-2 and B-2) are modified from Barth et al. (2024). Orange dots are reference points. A) Alpine Fault slip surface exposed at Hokuri Creek, looking NW (parts A-1, A-2). Lower hemisphere, equal-area stereogram (Part A-3) shows ~19 ± 2° of striation plunge variation for both the upper and lower track clusters (labelled in part A-2) due to their similar convex-downward shape. The tracks record northward rupture propagation at the site during a large (>3.5 m-long) slip event. B) Alpine Fault slip surface exposed at Martyr River, looking SE (parts B-1, B-2). For this direction of view, the local convex-upward curvature indicates northward rupture propagation. The enlarged image of part B-3 shows an individual slickenline track that is progressively deflected in a convex-upwards sense, whereas that of part B-4 shows an intersection between short tracks of differing plunge that can be attributed to this sense of overall slip curvature. C) Forward model from *Slicks* that can "explain" the basic slickenline pattern observed at Martyr River site, including inclined tracks overprinting older subhorizontal ones. An important feature of the model is a paucity of early-formed track inscriber nuclei at this site (blue dots), an abundance of neo-formed tracks, and their short average length. (For interpretation of the references to color in this figure legend, the reader is referred to the Web version of this article.)

surface, thus potentially complicating an interpretation of track curvature and rupture direction. Our kinematic modelling and observations of natural slickenlines on scarps of the Kekerengu Fault after the 2016 Kaikōura earthquake highlight several useful characteristics of curved slickenline patterns that might be used to interpret the direction of propagation of past earthquake ruptures. We have shown that the first-exhumed parts of natural scarps will preferentially expose and preserve curved tracks that formed early during the earthquake as a result of dynamic stress variations in the process zone of a propagating rupture. These sites include, for a strike-slip rupture, the leading edge of a lateral free face adjacent to an offset canyon wall, and for a dip-slip one, the upper part of a raised scarp. In the case of an oblique-slip rupture, both types of sites might exist in different places, depending on the topography. Using the shape of curved tracks to interpret rupture directivity requires the direction of view to be specified, because the direction of slip-path convexity flips from one fault block to the other (Fig. 4).

Many coseismic scarps, especially where overhanging, are gravitationally unstable. If a scarp collapses, curved striations of non-tectonic origin might be superposed into fault zone materials. In these situations, a local gravitational origin for slickenlines might be recognized by 1) identifying a landslide in the local geomorphology; and 2) recognizing late-formed striations that deflect downstream towards the downslope direction. In contrast to the curved striations generated by dynamic rupture stresses—which form early—gravitationally induced slip curvature should form late in the earthquake—or even after it. In other words, tectonic slickenlines should have curved upstream ends and straight downstream tails, whereas gravitational tracks should have the opposite shape.

Even where curvature cannot not be documented on long individual tracks; for example, in a case where most striae are straight and short, a second hallmark of curved slickenlines are intersections between adjacent tracks. The intersections involve older track segments with an "anomalous" plunge (relative to net-slip) that are cross-cut or overridden by younger ones having a plunge that is more representative of the overall fault kinematics (e.g., Fig. 4C, 8E and 9B). Importantly, striation intersections could easily be misinterpreted as evidence of multiple, linear slip events rather than of a single earthquake featuring a curved slip-path. Finally, even where no individual striation is seen to be curved and no intersections between striae are observed, a curved slip path might still be inferred on statistical grounds where mostly short, linear tracks are found to span a large range of individual pitch angles and/or directions, with a majority of them being subparallel to the total slip vector and a minority having an "anomalous" pitch. One could infer that the latter-mentioned striae formed during the early part of the slip path when the instantaneous slip direction was being most strongly deflected by dynamic stresses. By this reasoning, one could still use the overall striation pattern to infer the local sense of slip-path convexity and thus also the direction of rupture propagation (see inset box, Fig. 6D).

### 8.2. *Slickenline patterns as a potential record of changes in fault roughness*

Little is known about the roughness evolution of natural faults (Brodsky et al., 2011), and field studies of natural wear processes on fault exposures of spatial dimension similar to the slip magnitude are rare (Shervais and Kirkpatrick, 2016; Scholz, 2019). Experimental studies of faults are generally limited to a comparison of before and after views of the fault surface, with the intermediate steps being unobserved. Still less understood are changes in fault surface roughness that might take place at cm-meter scale during the course of a single earthquake. Our work suggests that analysing the shapes and lengths of slickenlines may provide insight into coseismic fault surface roughness evolution.

Our kinematic modelling shows how variation of two geometrical parameters relating to the durability ($P_1$) versus refreshment rate ($P_2$) of inscribing elements (asperities) on a fault can yield a diverse range of track patterns and track-length distributions. If a fault surface is dominated by an original (or early-formed) population of asperities, and only a few additional ones are added during the slip (i.e., case of a large $P_2$), then curved striae that record the early dynamic stress variation that took place in the process zone of the propagating rupture should be abundantly preserved on the scarp (Fig. 6C, E, and 6G). If the asperity destruction rate is low (i.e., their mean durability and longevity, $P_1$, is high), then many of the inscribed tracks will be long (equal to, or only slightly less than, the total slip), and their short, upstream curved segments will deflect downstream into longer, straight tails. Also, if there is a sufficient density of scribing elements, neighboring tracks will intersect one another (Fig. 6G). The corresponding track-length distributions will include a strong mode corresponding to the total slip magnitude (Fig. 7D). If the asperity destruction rate is high, then most of the tracks will be shorter than the total slip, early-formed, curved tracks will be more abundant than straight ones, and track intersections will be uncommon (Fig. 6C). Track-length distributions may be symmetrical or only slightly skewed towards the total slip distance (Fig. 7A, B, 7C).

By contrast to the above scenarios, if many new asperities nucleate afresh during the slip process to dominate the asperity population (low $P_2$), then curved striations will be uncommon and straight striation segments will dominate the population (Fig. 6D, F, and 6H). In this situation, If the asperity destruction rate is low (i.e, durability $P_1$ is high), then at least some long, partly curved tracks are likely be present as will track intersections, depending on the original density of asperities. The track-length distribution may feature a mode at the total slip distance (Fig. 7I and J). Alternatively, if the destruction rate is high (durability $P_1$ is low), then short tracks will predominate the population. Most will be straight, and few are likely to intersect (Fig. 6D). In the track-length distribution, a mode will probably not be present at the maximum slip distance, nor perhaps at any other length (Fig. 7F, G, and 7H).

We suggest that future studies might quantitatively analyze natural slickenline patterns and lengths to estimate $P_1$ and $P_2$ and perhaps their variances, values that will no doubt vary with lithology. In this way, new insight into the coseismic roughness evolution of fault surfaces at the mm-cm scale may be derived. Although they were not analyzed quantitatively, slickenlines inscribed on the Kekerengu Fault during the 2016 earthquake featured many curved or intersecting striations, as well as more abundant straight ones, with most tracks being $<0.5$ m long. These observations suggest that the fault surface was initially rough (i.e., many early-formed asperities and high $P_2$); and that these asperities were easily smoothed or removed during slip (i.e., low $P_1$, Fig. 6C). Put another way, during the earthquake an early-formed roughness was quickly removed and the fault became smoother. Presumably this process was accompanied by wear, leading to accumulation of the 1-2 cm-thick gouge layer.

Many previous studies have argued that faults generally get smoother with slip (e.g., Wesnousky, 1988; Sagy et al., 2007; Badt et al., 2016; Candela and Brodsky, 2016; Perrin et al., 2021). In detail, both smoothing and roughening of fault surfaces must occur, with the rates and mechanisms of these varying as a function of lithology, slip-rate, deformation conditions and spatial scale (e.g., Candela et al., 2012). Mechanical processes that can result in smoothing (i.e., asperity "deaths") include plucking, spalling or abrasion, plastic deformation (especially at $<1$ mm spatial scales), and the mantling of fault roughness by comminuted wear product (Candela and Brodsky, 2016; Shervais and Kirkpatrick, 2016; Scholz, 2019). In addition to these destructive mechanisms (especially in the near surface) an asperity might stop inscribing a track as a result of positive dilatation (opening up) of the fault caused by accumulation of porous wear product (e.g., Tesei et al., 2017) or by climbing of one asperity over another to prise apart the two walls of the fault (Candela et al., 2012; Kearse et al., 2019).

Our inference that the Kekerengu Fault surface initially roughened and then smoothed during the 2016 earthquake agrees with some studies documenting changes in fault surface roughness and wear at the

spatial scale of decimeters to a few meters (e.g., Brodsky et al., 2011). The thickness of comminuted fault rock that accumulates as a function of slip is typically thought to be dependent on normal stress, lithology (rock hardness), slip velocity and wear coefficient (Archard, 1953; Scholz, 2019). In formulas describing this relationship, the wear coefficient represents the probability of asperity removal per unit of slip. It is related to our asperity longevity parameter (Mean_Death_Age in Table 1), which is the numerator of durability parameter, $P_1$. Experimental studies at low confining pressure reveal the first few cm (<5) of fault slip is a peak-stress phase of initially very rapid wear and negative dilatation (possibly the result of asperity spalling and collapse) and striation incision. This high-stress phase is followed by an up to several meter-long "running-in" phase in which the shear stress falls, asperities continue to abrade or fail, the fault becomes smoother, and the wear rate tapers off towards a near steady-state value (Boneh et al., 2014; Davidesko et al., 2014; Badt et al., 2016). After this, cataclastic or intergranular flow of a continuous gouge layer (three-body mode) may dominate the rheology of the fault zone (Boneh et al., 2014; Brodsky et al., 2020). Depending on the rock type and local fluid conditions, the fault may then be healed or re-welded in the inter-slip period, later to be refractured and re-roughened by dynamic stresses and new fracturing at the inception of a new slip event (Klinger, 2010; Candela et al., 2012; Boneh et al., 2014)—and the cycle may repeat.

In contrast to smoothing, if many new asperities nucleate coseismically during slip then a fault may roughen as a function of slip. Providing a potential test for this, our modelling predicts that in this case curved slickenlines should be sparse, and most striations should be both straight and shorter than the total slip (Fig. 6D, F, and 6H). The corresponding track-length distribution might lack an obvious mode (Fig. 7F, G, 7H). In our models, such behaviour can be simulated by using a large value for the asperity birth-rate factor (parameter k in Table 1). Natural roughening mechanisms include the branching or splaying of faults due to dynamic stresses, new fracturing of a previously welded fault zone, secondary faults cross-cutting the main fault, and elastic interaction and linkage of originally separate fractures (Klinger, 2010; Candela et al., 2012; Boneh et al., 2014). Fracturing of locked asperities (or of the adjacent, highly stressed rock) may also increase roughness (e.g., Badt et al., 2016; Aslam and Daub, 2018). Roughening mechanisms most relevant to the cm-m scale of this study include the plucking of mm-scale grains. We have argued that dislodged fragments plucked from the wall of the Kekerengu Fault may have acted as plowing elements (Fig. 8F). Such clasts may be attached to neither fault block (third-body case) or alternately accrete to one of the fault blocks. In a similar way, a thickened packet of wear product may act as a third-body inscriber that simultaneously inscribes both blocks, or it may adhere onto one fault block to function as a new asperity there (Tesei et al., 2017; Brodsky et al., 2020).

## 9. Conclusions

Most slickenlines (slip striae) exposed on the scarps of historic earthquake ruptures are at least in part curved. These are thought to be inscribed during the earliest phase of slip as a result of dynamic stresses in the process zone of the propagating rupture. According to this model, the curved shape of the coseismic slip-path on a fault is governed by a site's location relative to the propagating rupture, the Andersonian faulting regime, and the fault friction parameters. Where documented, it can be used to infer the local direction of rupture propagation during a historic or paleo-earthquake.

The program *Slicks* simulates the shapes, orientations, lengths and topologies of curved to straight slickenline tracks that might form as the result of an earthquake of known slip mechanism and rupture propagation direction. The resultant geometrical patterns and length distributions of slickenline tracks are influenced by the total magnitude of slip, its early history of curvature, the initial density of scribing elements, and the statistical laws governing the relative rates of nucleation versus destruction of the fault surface asperities that inscribe tracks.

On a strike-slip rupture cutting incised topography, the leading edge of lateral free faces are likely to preserve curved slickenlines that formed early during the slip history. On a dip-slip rupture cutting flat ground, the exhumed scarp on the uplifted block is likely to preserve early-formed, curved tracks.

Where slickenline tracks are in part curved, they have the potential to intersect one another. These superpositions are not the result of multiple earthquake events but of changing directions of slip during a single event. The density of such intersections increases as the curvature of the slip-path increases, the total magnitude of slip (track length) increases, and the density of inscribers increases. Both the mean length of slickenline tracks and the frequency of their intersections increase as asperity durability increases. According to our simple models, curved tracks can only be inscribed by original or early-formed asperities. Completely straight tracks can only be inscribed by neo-formed ones.

As the durability of asperities increases, the mean length of tracks increases up to a maximum value, which is the total-slip distance. Where asperities are durable and long-lived, histograms of striation track length are likely to be asymmetric, with a mode corresponding to the total-slip distance. Such tracks also indicate the presence of original asperities present from the onset of slip. On the other hand, as the abundance of neo-formed (coseismically refreshed) asperities increases, the mean track length decreases.

Slickenline tracks observed on scarps of 2016 Kaikōura Earthquake had partially curved shapes with convexity directions matching those predicted by dynamic rupture models for direction of propagation and slip mechanism of that event. Further geometrical features of the slickenlines match the predictions of our kinematic models, such as the occurrence of track intersections (shallow-plunging tracks overprinting steeper ones) and curved slickenlines being especially common on the leading edge of lateral free faces.

Even without curved striations or track intersections, a curved slip path might still be inferred where mostly short, linear tracks span a large range of pitch angles, with a majority of them being subparallel to the total slip vector and a minority (presumably early-formed ones) having an "anomalous" pitch (relative to the net-slip) that reflects transient stress variation near the tip of the propagating rupture.

Analysing the shapes and lengths of slickenlines may provide new insight into coseismic fault surface roughness evolution, which is an elusive aspect of fault development during natural earthquakes. Striation patterns on the Kekerengu Fault suggest that many asperities were "born" at the beginning of the earthquake and that these were soon removed as the fault surface quickly smoothed during the coseismic slip.

## CRediT authorship contribution statement

**Timothy A. Little:** Writing – original draft, Visualization, Software, Methodology, Investigation, Funding acquisition, Formal analysis, Conceptualization. **Jesse Kearse:** Writing – review & editing, Validation, Methodology, Investigation. **Yoshi Kaneko:** Writing – review & editing, Methodology, Conceptualization. **Russ Van Dissen:** Writing – review & editing, Investigation, Funding acquisition.

## Declaration of competing interest

The authors declare that they have no known competing financial interests or personal relationships that could have appeared to influence the work reported in this paper.

## Acknowledgments

This work was funded by the Royal Society of New Zealand, Marsden Fund, grant number 20-GNS-006. We thank an anonymous reviewer for constructive comments.

## Appendix A. Supplementary data

Supplementary data to this article can be found online at https://doi.org/10.1016/j.jsg.2024.105291.

## Data availability

Data will be made available on request.

## References


Ando, R., Kaneko, Y., 2018. Dynamic rupture simulation reproduces spontaneous multifault rupture and arrest during the 2016 Mw 7.9 Kaikōura earthquake. Geophys. Res. Lett. 45 (12), 875–812,883.

Aoki, T., Koneko, Y., Kearse, J., 2023. Dynamic simulations of coseismic slickenlines on non-planar and rough faults. Geophys. J. Int. 233, 1124–1143.

Archard, J.F., 1953. Contact and rubbing of flat surfaces. J. Appl. Phys. 24, 981–988.

Aslam, K.S., Daub, E.G., 2018. Effect of fault roughness on aftershock distribution: elastic off-fault material properties. J. Geophys. Res. Solid Earth 123, 9689–9711.

Badt, N., Hatzor, Y.H., Toussaint, R., Sagy, A., 2016. Geometrical evolution of interlocked rough slip surfaces: the role of normal stress. Earth Planet Sci. Lett. 443, 153–161.

Barth, N., Kearse, J., Little, T.A., Van Dissen, R.J., 2024. Rupture direction of paleoearthquakes on the Alpine Fault, New Zealand, as recorded by curved slickenlines. Geology. https://doi.org/10.1130/G52543.52541.

Boneh, Y., Chang, J.C., Lockner, D.A., Reches, Z., 2014. Evolution of wear and friction along experimental faults. Pure Appl. Geophys. 171, 3125–3141.

Brodsky, E.E., Jacquelyn, J., Sagy, A., Colletini, C., 2011. Faults smooth gradually as a function of slip. Earth Planet Sci. Lett. 302, 185–193.

Brodsky, E.E., Kirkpatrick, J.D., Candela, T., 2016. Constraints from fault roughness on the scale-dependent strength of rocks. Geology 44, 19–22.

Brodsky, E.E., McLaskey, G.C., Ke, C.-Y., 2020. Groove generation and coelescence on a large-scale laboratory fault. AGU Advances 1, e2020AV000184.

Candela, T., Brodsky, E.E., 2016. The minimum scale of grooving on faults. Geology 44 (8), 603–606.

Candela, T., Renard, F., Kilinger, Y., Mair, K., Schmitt-buhl, J., Brodsky, E.E., 2012. Roughness of fault surfaces over nine decades of length scales. J. Geophys. Res. 117.

Cashman, P.H., Ellis, M.A., 1994. Fault interaction may generate multiple slip vectors on a single fault surface. Geology 22, 1123–1126.

Cesca, S., Zhang, Y., Mouslopoulou, V., Wang, R., Saul, J., Savage, M., Heimann, S., Kufner, S.K., Oncken, O., Dahm, T., 2017. Complex rupture process of the Mw 7.8, 2016, Kaikōura earthquake, New Zealand, and its aftershock sequence. Earth Planet Sci. Lett. 478, 110–120.

Davidesko, G., Sagy, A., Harzor, Y.H., 2014. Evolution of fault surface roughness through shear. Geophys. Res. Lett. 41 (5), 1492–1498.

DeMets, C., Gordon, R.G., Argus, D.F., Stein, S., 1994. Effect of recent revisions to the geomagnetic reversal time scale on estimates of current plate motions. Geophys. Res. Lett. 21, 2191–2194.

Doblas, M., 1998. Slickenside kinematic indicators. Tectonophysics 295 (1), 187–197.

Doblas, M., Rubio, J., 1987. Movimentos absolutas en fallas. Boletín Geológico y Minero de España 98 (IV), 493–506.

Holden, C., Kaneko, Y., D'Anastasio, E., Benites, R., Fry, B., Hamling, I.J., 2017. The 2016 Kaikōura earthquake revealed by kinematic source inversion and seismic wavefield simulations: slow rupture propagation on a geometrically complex crustal fault network. Geophys. Res. Lett. 44 (11), 320–311,328.

Howarth, J.D., Orpin, A.R., Kaneko, Y., Strachan, L.J., Nodder, S.D., Mountjoy, J.J., Bostock, H.C., Holden, C., Cağatay, M.N., 2021. Calibrating the marine turbidite palaeoseismometer using the 2016 Kaikōura earthquake. Nat. Geosci. https://doi.org/10.1038/s41561-41021-00692-41566.

Kaiser, A., Balfour, N., Fry, B., Holden, C., Litchfield, N., Gerstenberger, M., 2017. The 2016 Kaikōura, New Zealand, earthquake: preliminary seismological report. Seismol Res. Lett. 88, 727–739.

Kaneko, Y., Lapusta, N., Ampuero, J.P., 2008. Spectral element modeling of spantaneous earthquake rupture on rate and state faults: effect of velocity-strengthening friction at shallow depths. J. Geophys. Res. Solid Earth 113, B09317.

Kearse, J., 2018. Surface Fault Rupture and Slip Distribution of the Jordan-Kekerengu-Needles Fault Network during the 2016 Mw 7.8 Kaikōura Earthquake, New Zealand, School of Geography, Environment and Earth Sciences. Herenga Waka—Victoria University of Wellington, Wellington, New Zealand, p. 165.

Kearse, J., Kaneko, Y., 2020. On-fault geological fingerprint of earthquake rupture directions. J. Geophys. Res. Solid Earth 125 (9).

Kearse, J., Kaneko, Y., Little, T.A., Van Dissen, R.J., 2019. Curved slickenlines preserve direction of rupture propagation. Geology 47 (9), 838–842.

Kearse, J., Little, T.A., Van Dissen, R.J., Barnes, P., Langridge, R., Mountjoy, J., Ries, W., Villamor, P., Clark, K., Benson, A., Lamarche, G., Hill, M., Hemphill-Haley, M., 2018. Onshore to offshore ground surface and seabed rupture of the Jordan-Kekerengu-Needles fault network during the 2016, Mw7.8 Kaikoura earthquake, New Zealand. Bull. Seismol. Soc. Am. 108 (B3), 1573–1595.

Klinger, Y., 2010. Relation between continental strike-slip earthquake segmentation and thickness of the crust. J. Geophys. Res. 115 (115), B07306, 07310.01029/02009JB006550.

Litchfield, N.J., Villamor, P., Van Dissen, R.J., Nicol, A., Barnes, P., Barrell, D., Pettinga, J., others, 2018. Surface rupture of multiple crustal faults in the Mw 7.8 2016 Kaikōura, New Zealand, earthquake. Bull. Seismol. Soc. Am. 108 (B3), 1496–1520.

Macklin, C., Koneko, Y., Kearse, J., 2021. Coseismic slickenlines record the emergence of multiple rupture fronts during a surface-breaking earthquake. Tectonophysics 808, 228834.

Maerton, L., 2000. Variation in slip on intersecting normal faults: implications for paleostress inversion. J. Geophys. Res. 105 (B11), 25553–25565.

Mandal, N., Chakraborty, C., 1989. Fault motion and curved slickenlines: a theoretical analysis. J. Struct. Geol. 11 (4), 497–501.

Means, W.D., 1987. A newly recognized type of slickenside striation. J. Struct. Geol. 9 (5/6), 585–590.

Nicol, A., Howell, A., Litchfield, N., Wilson, T., Bannister, S., Massey, C., 2023. Introduction to the Kaikōura earthquake special issue. N. Z. J. Geol. Geophys. 66, 137–146.

Perrin, C., Waldhauser, F., Scholz, C.H., 2021. The shear deformation zone and the smoothing of faults with displacement. J. Geophys. Res. Solid Earth. 126 (5). https://doi.org/10.1029/2020JB020447.

Petit, J.P., 1987. Criteria for the sense of movement on fault surfaces in brittle rocks. J. Struct. Geol. 9 (5), 597–608.

Sagy, A., Brodsky, E.E., Axen, G.J., 2007. Evolution of fault surface roughness with slip. Geology 35, 283–286.

Scholz, C.H., 2019. The Mechanics of Earthquakes and Faulting, third ed. Cambridge University Press, Cambridge.

Shervais, K.A.H., Kirkpatrick, J.D., 2016. Smoothing and re-roughening processes: the geometric evolution of a single fault zone. J. Struct. Geol. 91, 130–143.

Somerville, P.G., Smith, N.F., Graves, R.W., Abrahamson, N.A., 1997. Modification of emperical strong ground motion attenuation relations to include the amplitude and duration effects of rupture directivity. Seismol Res. Lett. 68, 199–222.

Spudich, P., Guatteri, M., O'tuski, K., Minagawa, J.B.P.J., 1998. Use of fault striations and dislocation models to infer tectonic shear stress during the 1995 Hyogo-ken Nanbu (Kobe) earthquake. Bulletin of the Seismological Society of merica 88, 413–427.

Tesei, T., Carpenter, B.M., Giorgetti, C., Scuderi, M.M., Sagy, A., Scarlato, P., Collettini, C., 2017. Friction and scale-dependent deformation processes of large experimental carbonate faults. J. Struct. Geol. 100, 12–23.

Tjia, H.D., 2014. Fault-plane markings as displacement sense indicators. Indonesian Joiurnal of Earth Science 1 (3), 151–163.

Twiss, R.J., Gefell, M.J., 1990. Curved slickenfibers: a new brittle shear sense indicator with application to a sheared serpentinite. J. Struct. Geol. 12 (4), 471–481.

Wesnousky, S.G., 1988. Seismological and structural evolution of strike-slip faults. Nature 335, 340–342.

Wesnousky, S.G., 1989. Seismicity and the structural evolution of strike-slip faults. In: Schwartz, D.P., Sibson, R.H. (Eds.), Fault Segmentation and Controls of Rupture Initiation and Termination, pp. 409–425.

Xu, S., Nieto-Samaniego, A.F., Alaniz-Alvarez, S.A., 2013. Origin of superimposed and curved slickenlines in San Miguelito range, Central Mexico. Geol. Acta 11 (1), 103–112.

Xu, S.S., Nieto-Samaniego, A.F., Alaniz-Alvarez, S.A., Velasquillo-Matinez, L.G., 2011. Effect of block rotation of the pitch of slickenlines. Cent. Eur. J. Geosci. 3 (1), 29–36.